Cover statement:

Manuscript title: Replication timing maintains the global epigenetic state in human cells.
Author list: Kyle N. Klein, Peiyao A. Zhao, Xiaowen Lyu, Takayo Sasaki, Daniel A. Bartlett, Amar M. Singh, Ipek Tasan, Meng Zhang, Lotte P. Watts, Shin-ichiro Hiraga, Toyoaki Natsume, Xuemeng Zhou, Timour Baslan, Danny Leung, Masato T. Kanemaki, Anne D. Donaldson, Huimin Zhao, Stephen Dalton, Victor G. Corces, David M. Gilbert
Applicant role and contribution: I performed all computational methodology development and formal analyses for this manuscript. Together with Kyle (co-first author), Victor and David (two senior authors), we conceptualised and designed the study. I co-wrote the manuscript draft with Kyle.
Significance: DNA replication follows a highly regulated temporal order known as the DNA replication timing (RT) programme such that, in general, transcriptionally active chromatin is replicated early and inactive late. Early and late replication occur in different nuclear compartments established in the G1 phase. Widespread RT changes are triggered during cell fate changes and in disease. However, despite ample correlative observations, the functional significance of the RT programme has been a decades-long mystery. Given that chromatin is assembled at the replication fork, and different types of chromatin are assembled at different times during S phase, it is logical to assume that this programme is exploited to maintain epigenetic states within a cell type and alter them during cell fate transitions. However, there had been almost no direct evidence that the RT could influence chromatin composition and the chromatin architecture, with the exception of two publications from the Howard Cedar group in the late 2000s hinting at this possibility. One of the main hurdles is the robustness of the RT programme and the inability to manipulate it. Here we leveraged RIF1 knockout to abrogate the RT programme in human embryonic stem cells and investigated the epigenomic implications of global RT abrogation. Through a combination of molecular and computational approaches, we revealed RIF1's role in lowering replication stochasticity in the cell population. Its knockout caused dramatic increase in replication heterogeneity, which in turn caused genome-wide redistribution of histone modifications and consistent reorganisation of chromatin compartmentalization. We further confirmed the temporal order of events via conditional knockdown of RIF1 in cell cycle synchronised cell population. Our work here demonstrates that the RT programme is necessary for epigenome maintenance through successive cell cycles. This finding is impactful as it provides novel insights into the propagation of epigenetic memory and genome compartmentalization through cell cycles and opens up new mechanistic possibilities for understanding chromatin dysregulation in development and disease.

EPIGENOME

Replication timing maintains the global epigenetic state in human cells

Kyle N. Klein[1]†, Peiyao A. Zhao[1]†, Xiaowen Lyu[2,3]†, Takayo Sasaki[1,4], Daniel A. Bartlett[1], Amar M. Singh[5], Ipek Tasan[6], Meng Zhang[6], Lotte P. Watts[7], Shin-ichiro Hiraga[7], Toyoaki Natsume[8,9], Xuemeng Zhou[10], Timour Baslan[11], Danny Leung[10], Masato T. Kanemaki[8,9], Anne D. Donaldson[7], Huimin Zhao[6], Stephen Dalton[5], Victor G. Corces[2], David M. Gilbert[1,4]*

The temporal order of DNA replication [replication timing (RT)] is correlated with chromatin modifications and three-dimensional genome architecture; however, causal links have not been established, largely because of an inability to manipulate the global RT program. We show that loss of RIF1 causes near-complete elimination of the RT program by increasing heterogeneity between individual cells. RT changes are coupled with widespread alterations in chromatin modifications and genome compartmentalization. Conditional depletion of RIF1 causes replication-dependent disruption of histone modifications and alterations in genome architecture. These effects were magnified with successive cycles of altered RT. These results support models in which the timing of chromatin replication and thus assembly plays a key role in maintaining the global epigenetic state.

DNA is replicated during S phase of the cell cycle in a temporal order known as the replication timing (RT) program. RT is conserved among eukaryotes, is developmentally controlled, and correlates with many important epigenomic features (*1*). Early-replicating chromatin generally contains active histone modifications, is located in the nuclear interior, and correlates with the A compartment defined by high-throughput chromosome conformation capture (Hi-C) (*2*), whereas late-replicating chromatin is associated with transcriptionally repressive histone modifications, localization at the nuclear periphery, and the B compartment. Histone modifications are both recycled from parental chromatin and added de novo after passage of the replication fork, with different chromatin states showing differing dynamics of reassembly (*2*, *3*). Despite these close correlations, the mechanistic link between RT and the accurate maintenance of chromatin through cell cycles remains elusive. It has long been hypothesized that RT influences chromatin maintenance. Indeed, microinjection of plasmids into mammalian nuclei revealed that plasmids replicated in early S phase were decorated with acetylated histones, whereas those replicated later in S phase were devoid of acetylated histones (*4*, *5*). However, there is no direct evidence implicating RT in epigenetic state maintenance, largely because of the inability to manipulate genome-wide RT. The conserved protein RIF1 has been shown to affect RT in many eukaryotes; however, because the effects have been partial or localized, RIF1 disruption has not been exploited to study the effects of RT abrogation (*6*, *7*).

[1]Department of Biological Science, Florida State University, Tallahassee, FL 32306, USA. [2]Department of Human Genetics, Emory University School of Medicine, Atlanta, GA 30322, USA. [3]State Key Laboratory of Cellular Stress Biology, Fujian Provincial Key Laboratory of Reproductive Health Research, School of Medicine, Xiamen University, Xiamen, China. [4]San Diego Biomedical Research Institute, La Jolla, CA 92121, USA. [5]Department of Biochemistry and Molecular Biology, University of Georgia, Athens, GA 30602, USA. [6]Department of Chemical and Biomolecular Engineering, University of Illinois at Urbana-Champaign, Urbana, IL 61801, USA. [7]Institute of Medical Sciences, University of Aberdeen, Aberdeen AB25 2ZD, UK. [8]Department of Chromosome Science, National Institute of Genetics, Research Organization of Information and Systems (ROIS), Yata 1111, Mishima, Shizuoka 411-8540, Japan. [9]Department of Genetics, The Graduate University for Advanced Studies (SOKENDAI), Yata 1111, Mishima, Shizuoka 411-8540, Japan. [10]Division of Life Science, Hong Kong University of Science and Technology, Clear Water Bay, Hong Kong, China. [11]Cancer Biology and Genetics Program, Memorial Sloan Kettering Cancer Center, New York, NY 10065, USA.
*Corresponding author. Email: gilbert@sdbri.org
†These authors contributed equally to this work.

RIF1 knockout causes heterogeneous RT

To gain insight into the role of genome-wide RT in shaping the epigenome, we knocked out RIF1 (RIF1 KO) in H9 human embryonic stem cell (hESC), HCT116 (fig. S1, A to C), and HAP1 cell lines (supplementary methods). As previously reported (*8*), all three RIF1 KO cell lines proceeded through the cell cycle with nearly wild-type (WT) kinetics (fig. S1, D and E) and exhibited genome-wide aberrations in RT, albeit with varying degrees of severity (Fig. 1A). Similar to prior reports in mammalian cells (*6*), domains changed RT from either early to late (EtL) or late to early (LtE) in log2(E/L) RT profiles of HCT116 and HAP1 cells. RIF1 KO caused 43% of the genome to change RT in HCT116 cells (23% EtL and 20% LtE) and 39% of the genome to change in HAP1 cells (20% EtL and 19% LtE) (fig. S1F). However, in H9 hESCs (Fig. 1A), nearly the entire genome acquired a log2(E/L) close to zero (fig. S1F). RIF1 control of RT in hESCs was dosage dependent, because partial knockdown (KD) of RIF1 in H9 hESCs (fig. S2A) resulted in a partial effect on the RT program (fig. S2, B and C). Replication foci (*9*) in RIF1 KO cells showed a "blending" of early and middle spatial patterns (fig. S3). These results demonstrate a considerably more extensive role for RIF1 in RT control in hESCs than in other cell types.

Previous reports have interpreted RT changes in RIF1 KO cells as distinct RT switches (*6*), but the severity of the RT phenotype in RIF1 KO hESCs suggested an alternative mechanism. To address this, we performed high-resolution Repli-seq (*10*) (fig. S4A) in RIF1 KO cells, which identifies peaks of replication initiation termed initiation zones (IZs) and valleys of late replication containing broadly distributed, low-efficiency initiation events (*10*). We detected dramatic diffusion of RT patterns and loss of defined IZs in both HCT116 and H9 hESCs (Fig. 1B and fig. S4B), indicating major RT variation within the cell population (fig. S4, C and D). Most notably, there was a nearly complete genome-wide abrogation of the RT program in RIF1 KO H9 hESCs (Fig. 1B and fig. S4B). In RIF1 KO HCT116 cells, EtL and LtE regions called using E/L Repli-seq showed substantial loss of temporal control (fig. S4, E and F). Even early regions that were not called as EtL switches in E/L Repli-seq lost defined patterns (compare Fig. 1, A and B, with fig. S4, E and F), indicating that the entirety of the early-replicating genome lost RT control upon RIF1 KO in both cell lines. By contrast, many late-replicating regions in HCT116 retained late replication (fig. S4, E and F), indicating a RIF1-independent mechanism controlling RT for these regions. We next divided each IZ called in WT high-resolution Repli-seq into four S-phase timing classes (*10*) and plotted the cumulative percentage of DNA replicated through S phase (Fig. 1C). WT cells showed typical segregation of IZs according to the temporal order (*10*), whereas RIF1 KO cells showed major overlap of IZ classes and flatter sigmoidal-like curves (Fig. 1C). We subsequently calculated the genome-wide heterogeneity parameter T_{width}, which is positively correlated with heterogeneity. We found that genome-wide T_{width} was greatly increased in both cell types upon RIF1 KO (fig. S4G), indicating a significant increase in RT heterogeneity.

To directly validate increased cell-to-cell RT heterogeneity in RIF1 KO, we performed single-cell Repli-seq (*11*) on WT and RIF1 KO HAP1 cells. RIF1 KO cells showed co-replication of early and late domains (fig. S5) and had a notably larger T_{width} compared with WT cells (Fig. 1D), directly confirming that RIF1 KO disrupts RT by substantially increasing RT heterogeneity rather than causing discrete RT shifts in all cells.

RIF1 KO alters distribution of heterochromatic histone modifications

To map RIF1 binding, we performed Cut&Run (cleavage under targets and release using nuclease) against green fluorescent protein (GFP)

on GFP-tagged RIF1 in HCT116 and H9 hESCs (fig. S6A). RIF1 was enriched in the late-replicating portion of the genome in both cell lines (fig. S6, B and C) and bound chromatin in broad domains (Fig. 2A). In both cell lines, RIF1 binding was enriched at regions that lost RT control upon RIF1 KO (affected regions) (Fig. 2, A, B, and E; and fig. S6, D to F), whereas those regions that maintained their late RT (unaffected regions) had low RIF1 enrichment (Fig. 2, C, D, and E; and fig. S6, D and E). However, in RIF1 KO H9 hESCs, the regions defined as "unaffected regions" are rare and still display RT dysregulation but significantly less than "affected regions" (Fig. 2, compare D with B).

We next performed chromatin immunoprecipitation combined with sequencing (ChIP-seq) (spike-in) on the late replication–associated histone mark H3K9me3 (histone 3 lysine 9 trimethylation) in RIF1 KO cells (fig. S7). In WT cells, affected regions were enriched for smaller H3K9me3 peaks, whereas unaffected regions contained large H3K9me3 domains (Fig. 2, A, C, and E; and fig. S8, A and B). In HCT116, small H3K9me3 peaks at affected regions (n = 390) were lost (Fig. 2, A and E), and the large H3K9me3 domains at unaffected regions (n = 209) were strengthened (Fig. 2, C and E). H3K9me3 was globally depleted in H9 hESCs (fig. S8, C and D). The rare unaffected domains in RIF1 KO H9 hESCs (n = 49) were large H3K9me3 domains that were only slightly diminished for H3K9me3 compared with affected domains (Fig. 2E). Unaffected H3K9me3 domains did not overlap greatly between cell types (fig. S8E). H3K9me3 depletion in HCT116 RIF1 KO cells (fig. S8F) caused partial earlier replication of unaffected regions (Fig. 2F and fig. S8, G and H), indicating a role for H3K9me3 in their late replication but implicating additional unknown mechanisms [possibly association with the nuclear lamina (*8*)] in maintaining late RT at unaffected regions. By contrast, RIF1 KO caused cell type–specific changes to H3K27me3 (histone 3 lysine 27 trimethylation), with H9 hESCs primarily exhibiting down-regulation and HCT116 exhibiting overall up-regulation (fig. S9). These results reveal that multiple mechanisms, including RIF1 and large H3K9me3 domains, orchestrate late RT to different extents in different cell types.

Affected and unaffected late-replicating regions form separate interaction hubs

The strong association between late replication and B compartmentalization (*12*) compelled us to investigate the genomic compartmentalization of RIF1 KO cells by Hi-C. Notably, we found that affected and unaffected regions had distinct PC1 eigenvector associations despite being similarly late-replicating in WT cells, and this distinction was increased upon RIF1 KO (fig. S10A). WT interactions between unaffected regions were significantly stronger than interactions between affected regions or those between unaffected regions and affected regions (fig. S10B). Upon RIF1 KO, unaffected regions formed new interactions and strengthened existing interactions (Fig. 2G and fig. S10C). Strengthened interactions were correlated with up-regulated H3K9me3 domains (fig. S10D). We then sorted affected and unaffected regions according to the extent of H3K9me3 changes [negative (down-regulated) or positive (up-regulated)] and calculated their interaction frequencies. In WT cells, up-regulated and down-regulated H3K9me3 peaks formed separate interaction hubs (Fig. 2H, left

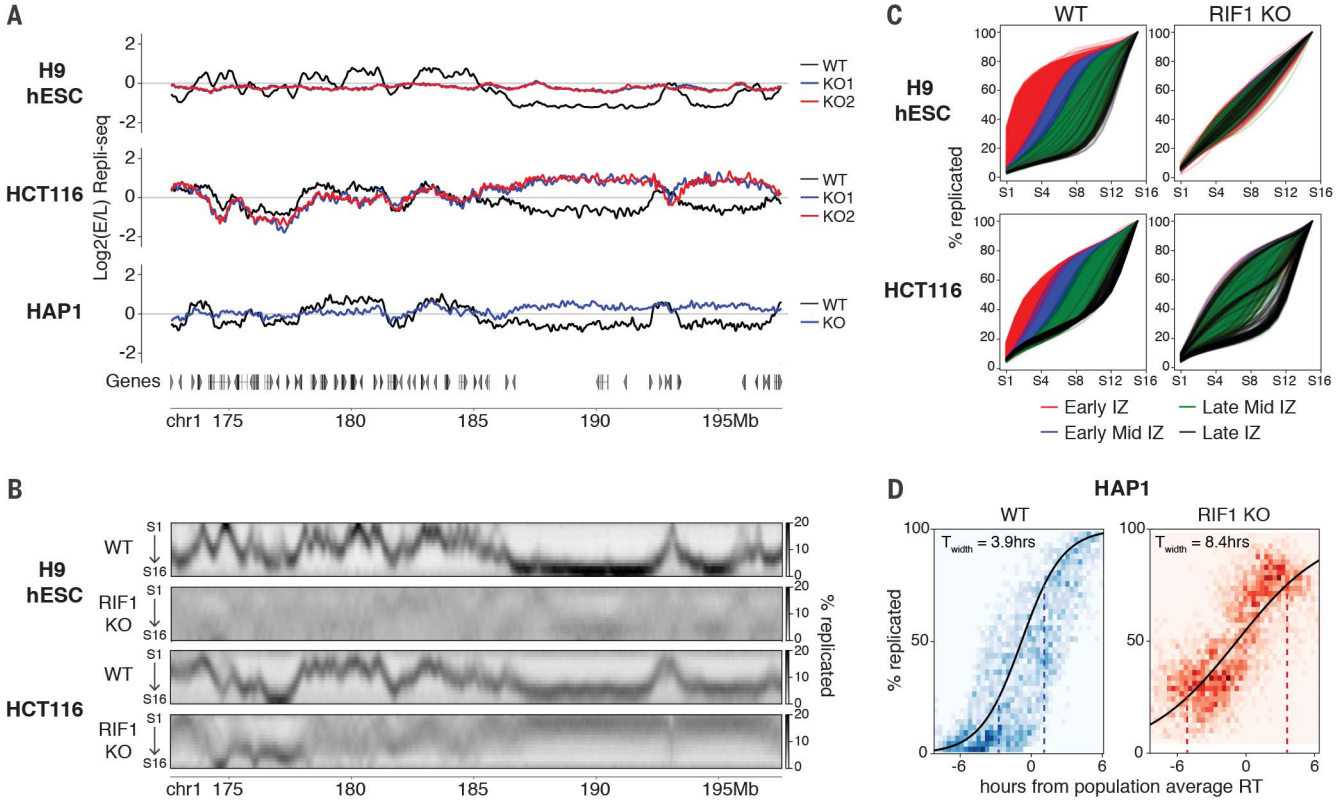

Fig. 1. RIF1 controls RT by reducing cell-to-cell variation in replication timing. (**A**) Log2(E/L) Repli-seq plots of chromosome 1 (Chr1), 172.6 to 197.6 Mb, in WT (black) and two RIF1 KO clones (blue and red) in H9 hESC (top), HCT116 (middle), and HAP1 (bottom) cell lines. (**B**) High-resolution Repli-seq plots of Chr1 172.6 to 197.6 Mb in WT and RIF1 KO in H9 hESCs (top two) and HCT116 (bottom two); same locus as in (A). (**C**) Cumulative percentage of replicated plots for each IZ called in WT cells versus S-phase fraction of 16-fraction Repli-seq, color-coded by their timing (red, early; blue, early middle; green, late middle; black, late). (**D**) Sigmoidal fitting of the percentage of cells having replicated in each bin (y axis) against time in hours from population average RT (x axis) for HAP1 WT (left) and RIF1 KO (right). The heatmaps (blue, WT; red, KO) represent the data spread for all 50-kb bins genome-wide in all single cells (51 WT and 69 KO). Dotted lines at 25% of cells replicated and 75% of cells replicated indicate the span of T_{width}.

column) that were strengthened and weakened, respectively, upon RIF1 KO (Fig. 2H, right column), accentuating the separation between the two. In individual cases, the juxtaposition of affected and unaffected domains created new compartment and topologically associating domain (TAD) boundaries (fig. S10, E and F). These results demonstrate that affected and unaffected H3K9me3 regions are two intrinsically different classes of late-replicating chromatin with distinct interaction preferences; unaffected domains form strong interactions with one another to form a compartment that maintains late RT without RIF1, whereas affected domains form a separate hub of

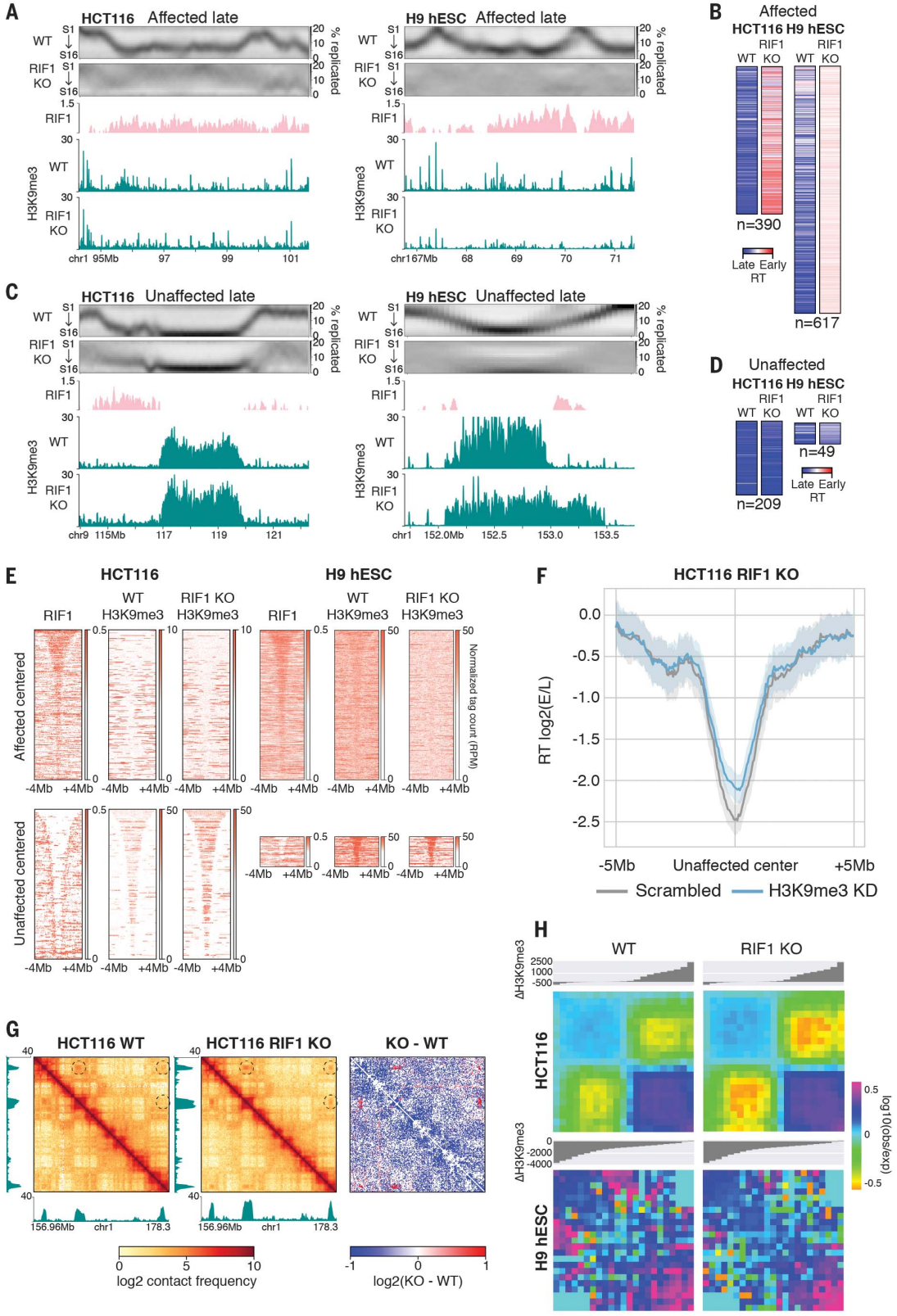

Fig. 2. RT affected and unaffected late regions are distinct classes of chromatin. (**A**) Affected late region at Chr1 94.3 to 101.6 Mb in HCT116 (left) and Chr1 66.75 to 71.4 Mb in H9 hESCs (right) showing, from top to bottom, high-resolution Repli-seq in WT and RIF1 KO cells, RIF1 fold enrichment in WT cells, and H3K9me3 ChIP-seq tag counts in WT and RIF1 KO cells. (**B**) Heatmaps of RT indices for affected late regions in WT and RIF1 KO of HCT116 and H9 hESCs. (**C**) Unaffected late region at Chr9 113.95 to 122.3 Mb in HCT116 (left) and Chr1 151.7 to 153.75 Mb in H9 hESCs (right), displayed as in (A). (**D**) Heatmaps of RT indices for unaffected late regions in WT and RIF1 KO of HCT116 and H9 hESCs. (**E**) RIF1 and H3K9me3 binding in HCT116 (left) and H9 hESC (right) WT or RIF1 KO cells centered on affected late regions (top) or unaffected late regions (bottom) ±4 Mb and sorted by size. (**F**) Mean log2(E/L) Repli-seq scores centered at all unaffected late regions ±5 Mb in HCT116 RIF1 KO transfected with scrambled control (gray) or H3K9me3 KD (blue) small interfering RNA. Shadow represents 95% confidence interval. (**G**) H3K9me3 tag count tracks beside ICE (iterative correction and eigenvector decomposition)–normalized Hi-C and subtraction contact maps of HCT116 WT and RIF1 KO at Chr1 156.95 to 178.3 Mb. Dotted circles denote regions of increased interaction. (**H**) Log10(observed/expected) aggregate interactions between late regions in WT and RIF1 KO HCT116 (top) and H9 hESCs (bottom). The interactions were binned into 11 equal segments, which were ranked by increasing ΔH3K9me3, where negative and positive values indicate, respectively, decreased and increased H3K9me3 in RIF1 KO compared with WT.

interactions and require RIF1 to enforce late replication.

RIF1 KO causes depleted active histone modifications and attenuated A compartment interactions

ChIP-seq of H3K27ac (histone 3 lysine 27 acetylation) (spike-in) and H3K4me3 (histone 3 lysine 4 trimethylation) revealed that both marks became depleted in both RIF1 KO cells (figs. S7 and S11, A to C). Loss of active marks from the A compartment was concurrent with changes in compartmentalization and Hi-C interactions in both cell lines. In H9 hESCs, the majority of compartment changes involved the disappearance of A compartment chromatin into neighboring B compartments (Fig. 3, A and B; and fig. S11D), whereas HCT116 exhibited discrete shifts in compartmentalization in both directions (Fig. 3A and fig. S11, D and E). Loss of A compartment interactions in Hi-C contact maps corresponded to reduced H3K27ac peaks in both cell lines [Fig. 3C inset (arrows) and fig. S11F (arrows)]. Within A-to-B compartment switches, the levels of H3K27ac and H3K4me3 were significantly depleted (Fig. 3D), and the interactions between H3K27ac peaks were reduced

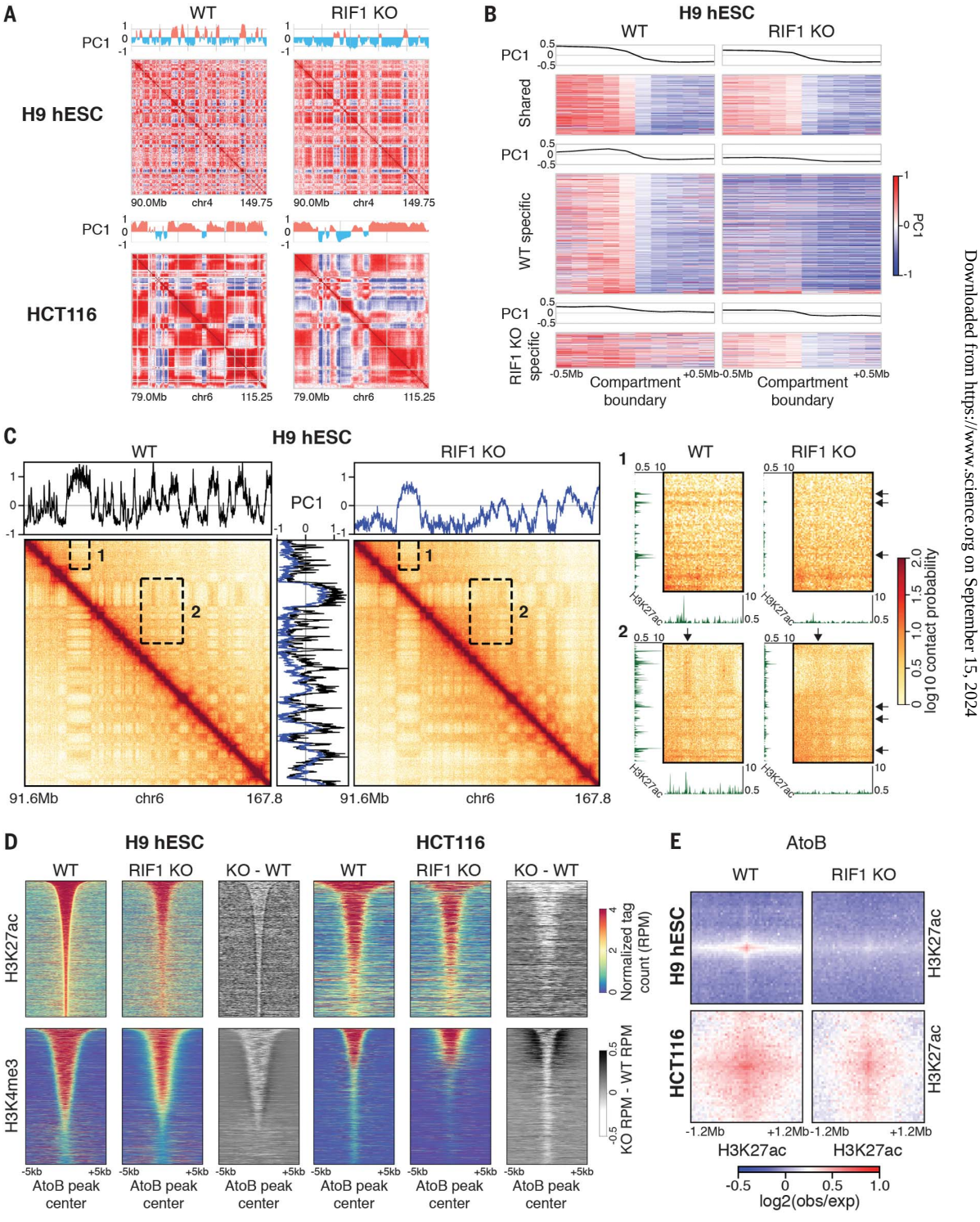

Fig. 3. RIF1 KO causes global alterations of compartments and epigenetic state. (**A**) Correlation matrices and PC1 eigenvector of Chr4 90.0 to 149.75 Mb in WT and RIF1 KO H9 hESCs (top) and Chr6 79.0 to 115.25 Mb in WT and RIF1 KO HCT116 (bottom). (**B**) Heatmaps of PC1 values centered on shared (top), WT-specific (middle), and RIF1 KO–specific (bottom) compartment boundaries ±0.5 Mb in WT and RIF1 KO H9 hESCs. (**C**) ICE-normalized Hi-C contact map of Chr6 91.6 to 167.8 Mb in H9 hESC WT and RIF1 KO cells with accompanying PC1 eigenvector plots (black, WT; blue, KO). To the right are expanded views of insets 1 and 2 with accompanying H3K27ac ChIP-seq plots. Arrows indicate compartments and ChIP-seq peaks that are lost upon RIF1 KO. (**D**) Normalized tag counts [reads per million (RPM)] of signal and subtraction plots for H3K27ac and H3K4me3 centered on peaks within A-B compartment-switching regions ±5 kb in WT and RIF1 KO cells sorted by peak size. (**E**) Aggregate Hi-C log2(observed/expected) interactions between H3K27ac peaks within A-B compartment-switching regions ±1.2 Mb in WT and RIF1 KO cells.

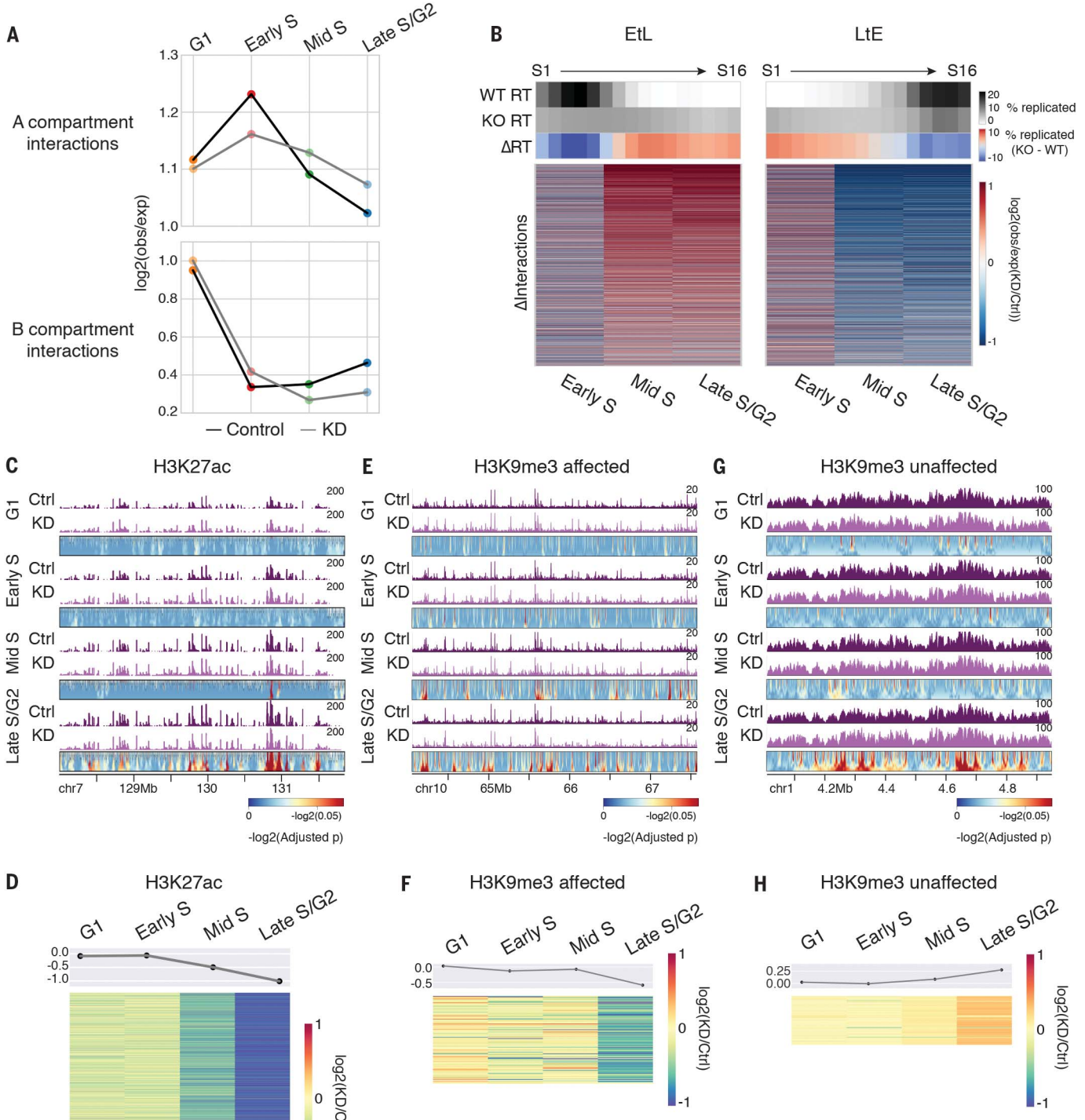

Fig. 4. Epigenome effects require DNA replication and occur during the first S phase after RIF1 degradation. (**A**) Average log2(observed/expected) within the top 10% A (top) and B (bottom) compartments in control (black line) and RIF1 KD (gray line) cells at G_1, early S, middle S, and late S/G_2 time points. (**B**) Interaction frequency differences between control and RIF1 KD at top 10% EtL and LtE regions at G_1, early S, middle S, and late S/G_2 time points whose RT is indicated by average high-resolution Repli-seq heatmaps. (**C**) H3K27ac ChIP-seq of Chr7 128 to 131.9 Mb in control (top), RIF1 KD (middle), and domainogram (bottom), indicating −log2 (Benjamini-Hochberg–adjusted *P* values) calculated for the differences of control subtracted from KD tracks (supplementary methods). (**D**) Heatmap showing log2(KD/control) of H3K27ac peaks. (**E**) H3K9me3 ChIP-seq of Chr10 64.05 to 67.6 Mb in control (top), RIF1 KD (middle), and domainogram (bottom). (**F**) Heatmap showing log2(KD/control) of H3K9me3 peaks at affected regions. (**G**) H3K9me3 ChIP-seq of Chr1 4.05 to 5.0 Mb in control (top), RIF1 KD (middle), and domainogram (bottom). (**H**) Heatmap showing log2(KD/control) of H3K9me3 domains at unaffected regions.

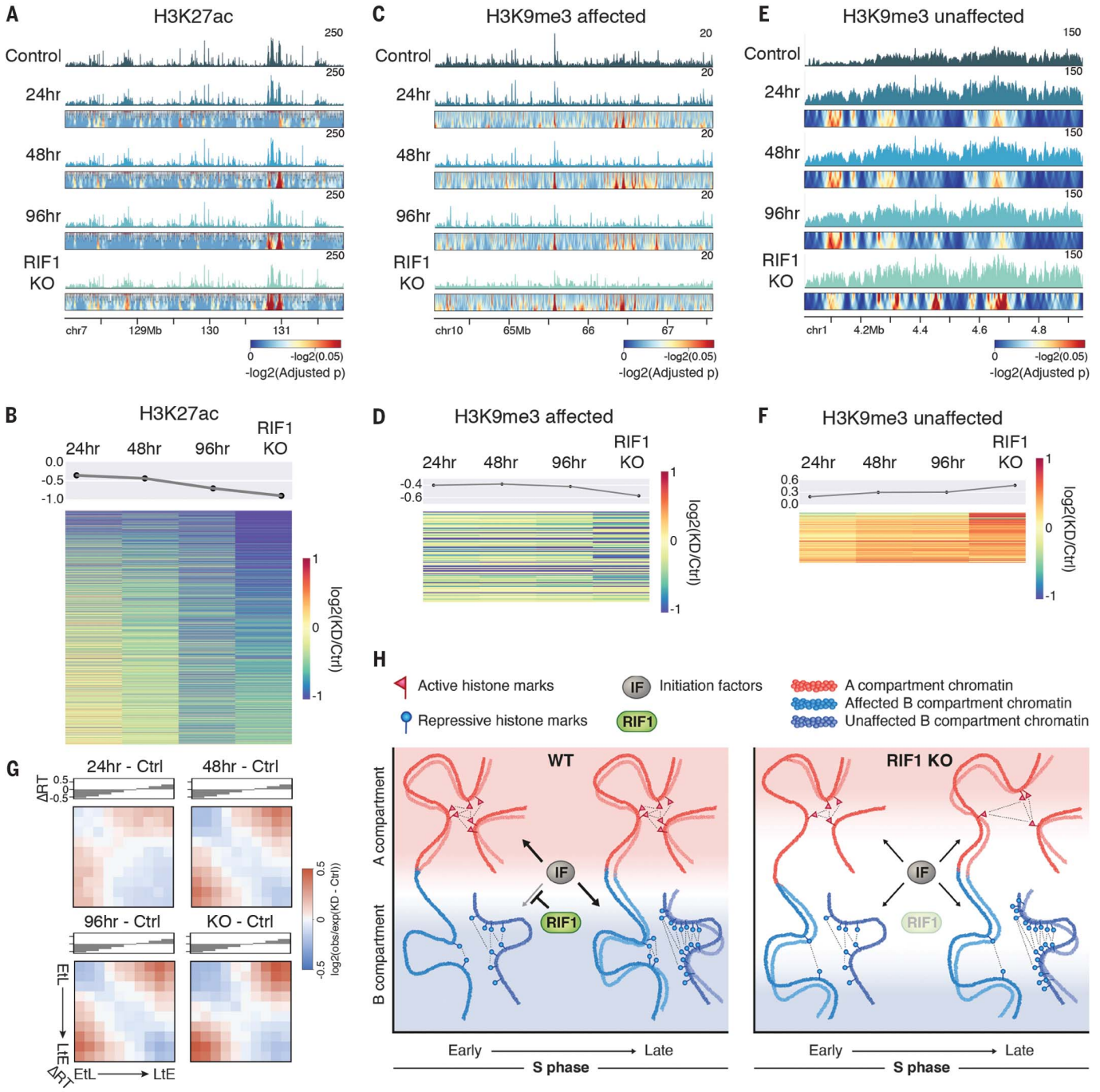

Fig. 5. Epigenome effects are exacerbated as cells cycle without RT control. (**A**) H3K27ac ChIP-seq of Chr7 128 to 131.9 Mb in control (top), RIF1 KD (middle), and domainograms (bottom) in controls, after 24, 48, or 96 hours of degradation, and RIF1 KO. (**B**) Heatmap showing log2(KD/control) of H3K27ac tags. (**C**) H3K9me3 ChIP-seq of Chr10 64.05 to 67.6 Mb in control (top), RIF1 KD (middle), and domainograms (bottom). (**D**) Heatmap showing log2(KD/control) of H3K9me3 tags at affected regions. (**E**) H3K9me3 ChIP-seq of Chr1 4.05 to 5.0 Mb in control (top), RIF1 KD (middle), and domainograms (bottom). (**F**) Heatmap showing log2(KD/control) of H3K9me3 tags at unaffected regions. (**G**) Subtraction saddle plots of cis-log2(observed/expected) contacts of control sample from 24, 48, and 96 hours of degradation, and RIF1 KO sorted by ΔRT (KD RT − control RT). (**H**) Working model illustrating the role of RT in epigenome maintenance. In WT cells, RIF1 prevents replication initiation factors from activating replication within repressive chromatin, allowing early replication of active chromatin, which is then assembled with active histone marks (red flags) that self-interact to form the A compartment. Repressive chromatin is replicated in late S phase and is assembled with repressive histone marks (blue circles), which self-interact to form the B compartment. The B compartment is divided into regions that depend on RIF1 for late replication (affected) and those that do not (unaffected). RIF1 KO allows limiting replication initiation factors to associate heterogeneously with both active and repressive chromatin, delaying replication of the former and advancing replication of the latter. Delayed replication of active chromatin causes depletion of active histone marks and weakens interactions within the A compartment. Advanced replication of affected repressive chromatin causes depletion of repressive histone marks and weakens interactions within the affected B compartment hub. Unaffected B compartment hubs associated with repressive domains maintain their late replication in RIF1 KO and become enriched for repressive histone marks.

(Fig. 3E). These data show that depletion of active histone modifications, particularly H3K27ac, strongly correlates with loss of A compartment interactions in RIF1 KO cells.

Both cell lines exhibited genome-wide weakening of A-A compartment interactions that was accompanied by strengthening of B-B compartment interactions (fig. S12A). This was further confirmed when we called statistically significant differential interactions using differential Hi-C. Strengthened interactions were seen predominantly within the B compartment and weakened interactions were concentrated in the A compartment in both cell lines (fig. S12, B and C). This is likely the combined effect of strengthened interactions between up-regulated H3K9me3 domains within the B compartment (fig. S12D) and weakened interactions between down-regulated H3K27ac peaks in the A compartment (fig. S12E) and suggests a redefining of compartment identities in RIF1 KO cells. EtL and LtE regions showed occasional loss and gain of TAD boundaries, respectively (fig. S13A). However, globally, the positioning and number of TAD boundaries was not significantly affected by RIF1 KO in either cell line (fig. S13B), whereas the strength of TAD boundaries was increased (fig. S13, C and D), independent of RAD21 binding (fig. S14). Together, these data indicate a substantial reorganization of genomic compartments that correlates with epigenome changes in RIF1 KO cells.

DNA replication is required for epigenomic changes

To directly address the primary role of RIF1, we used an auxin-inducible degron (AID) system (*13*) in HCT116 cells to rapidly degrade RIF1 (fig. S15A). We first confirmed that RT defects observed in RIF1 KO occur during the first S phase after RIF1 loss (fig. S15, B and C) by degrading RIF1 in G_1-synchronized cells and performing E/L Repli-seq upon release into S phase. We next synchronized cells in G_1, degraded RIF1, either held them in G_1 or released them into early, middle, or late S phase/G_2 (fig. S15, D and E), and performed Hi-C and ChIP-seq. We found no notable difference in genome organization between RIF1 degraded and control cells held in G_1 (Fig. 4A and fig. S16, A to F). We observed extensive architectural changes at both A and B compartment chromatin as control cells transitioned from G_1 into and through S phase (Fig. 4A and fig. S16, A to F), controlled for copy number (fig. S16G), and this was characterized by an initial increase and subsequent decrease in interaction frequencies within A compartment and the converse within B compartment regions (Fig. 4A, control lines). RIF1 KD cells showed diminished dynamics with decreased intra-A interactions and increased intra-B interactions during early S phase and the reverse during middle and late S phase compared with control cells (KD lines in Fig. 4A and fig. S16, C to F). These changes were coincidental with RT disruptions at corresponding loci (Fig. 4B and fig. S16H). These results demonstrate that RIF1 is required for extensive architectural changes during S phase, suggesting that these changes are linked to the normal temporal order of replication.

H3K27ac and H3K9me3 ChIP-seq (spike-in) also revealed no significant difference between RIF1 degraded and control cells held in G_1 (G_1 data in Fig. 4, C to H; and fig. S17, A and B), indicating that histone mark changes are also not a direct result of RIF1 loss. H3K27ac peaks were not depleted until cells reached middle S phase with the extent of depletion greatest at late S phase [Fig. 4, C and D; and fig. S17, A (blue dots) and C], suggesting that disruption of early-enriched histone marks takes place only when they are replicated late. H3K9me3 peaks at affected regions became depleted in late S/G_2 [Fig. 4, E and F; and fig. S17, B (blue dots) and D], whereas H3K9me3 domains at unaffected regions became more enriched for H3K9me3 at late S phase/G_2 [Fig. 4, G and H; and fig. S17, B (red dots) and E]. Together, these results indicate that disruption of genomic structure and chromatin identity in RIF1 degraded cells is a result of a dysregulated DNA replication program.

Epigenomic changes are quantitatively correlated with lengths of RT dysregulation

We further hypothesized that extended degradation of RIF1 and RT disruption through multiple rounds of DNA replication would exacerbate the observed epigenomic phenotypes. To test this, we degraded RIF1 for 24, 48, and 96 hours (fig. S18A), constituting ~1, 2, and 4 cell cycles respectively. After 24 hours of RIF1 degradation, the RIF1 KO RT phenotype was fully recapitulated and remained so throughout the time course (fig. S17, B and C). H3K27ac peaks that were depleted in RIF1 KO cells, and the interactions between them, progressively diminished toward RIF1 KO levels with time (Fig. 5, A and B; and fig. S18, D to F). H3K9me3 peaks at affected late-replicating regions became significantly depleted after 24 hours of RIF1 degradation and remained depleted throughout the time course [Fig. 5, C and D; and fig. S18, G and H (blue dots)]. Unaffected regions progressively accumulated H3K9me3 throughout the time course [Fig. 5, E and F; and fig. S18, H (red dots) and I]; however, the strengthening of interactions between H3K9me3 domains seen in RIF1 KO was not observed even after 96 hours of RIF1 degradation (fig. S18J). Sorting chromatin interactions by the change in RT (ΔRT) revealed that regions that changed RT (both EtL and LtE) gradually lost interactions with regions of normally similar RT (upper left and lower right corners of Fig. 5G) and gained interactions with regions of normally different RT (upper-right and lower-left corners of Fig. 5G), indicating a strong correlation between RT loss and disruption of chromatin contacts. Together, these data show that as cells progress through multiple rounds of DNA replication with dysregulated RT, they gradually accumulate aberrant epigenomic and structural signatures, supporting the model that stochastic RT gradually affects newly synthesized chromatin with each round of mistimed chromatin assembly.

RIF1 KO causes limited gene expression changes

RIF1 KO caused expression changes to 2284 genes in H9 hESCs and 1737 genes in HCT116 (fig. S19, A and B) as well as to some endogenous retrovirus (ERV) elements (fig. S19C). Expression of pluripotency factors or histone modification writers was not affected (fig. S19D). Genes affected in HCT116 RIF1 KO gradually changed their expression during the RIF1-AID degradation time course toward RIF1 KO levels (fig. S19E); however, only six significantly changed genes were shared between all RNA sequencing (RNA-seq) samples (fig. S19F and table S1). Single-cell RNA-seq revealed an increase in global cell-to-cell heterogeneity in gene expression in RIF1 KO H9 hESCs and HAP1 cells but not HCT116 (fig. S19, G to I).

RT and chromatin compartmentalization are correlated with gene expression (*1*); however, neither changes in RT nor compartment switches were able to predict gene expression changes in RIF1 KO cells (fig. S20, A to D). Differentially expressed genes showed cell type–specific changes in the distribution of specific histone modifications around their transcription start sites that correlated with expression changes (fig. S20, E and F). Altogether, these results suggest that gene expression changes are indirect effects of RIF1 depletion.

Discussion

We show that deletion of RIF1 results in a dramatic increase in cell-to-cell RT heterogeneity rather than discrete population-level RT switches. Although RIF1 is bound to late-replicating chromatin, the entire early-replicating genome as well as most of the late-replicating genome becomes disrupted for RT control without RIF1 (Fig. 1). This is reminiscent of observations in budding yeast, where derepression of late-replicating origins increased competition for limiting replication initiation factors and delayed the RT of early origins (*14*), and it suggests a similar mechanism of RT disruption in RIF1 KO cells. The late-replicating genome is composed of two types of domains whose delayed replication is enforced by different mechanisms and that form separate chromatin hubs. In both hESCs and HCT116 cells, RIF1 KO leads to widespread aberrant

histone modification patterns that correlate with distinct genome-wide changes in three-dimensional genome architecture. We further show that disruptions to epigenome and chromatin structure require DNA replication and that continuous rounds of replication with heterogeneous RT quantitatively exacerbate these changes. We propose that RT changes due to RIF1 KO result in aberrant reestablishment of epigenetic marks that cause profound changes in the epigenetic landscape that then alter genome architecture (Fig. 5H). Although mouse RIF1 has been shown to interact with histone methytransferases (*15*), our cell cycle–synchronized data (Fig. 4) do not support a direct role for RIF1 in heterochromatin maintenance. This work provides mechanistic evidence linking the RT program with maintenance of the global epigenetic state and genome compartmentalization and establishes RIF1 as a key regulator of epigenome maintenance through its role in RT control.

REFERENCES AND NOTES

1. N. Rhind, D. M. Gilbert, *Cold Spring Harb. Perspect. Biol.* **5**, a010132 (2013).
2. N. Reverón-Gómez *et al.*, *Mol. Cell* **72**, 239–249.e5 (2018).
3. T. M. Escobar *et al.*, *Cell* **179**, 953–963.e11 (2019).
4. J. Zhang, F. Xu, T. Hashimshony, I. Keshet, H. Cedar, *Nature* **420**, 198–202 (2002).
5. L. Lande-Diner, J. Zhang, H. Cedar, *Mol. Cell* **34**, 767–774 (2009).
6. S. B. C. Buonomo, in *DNA Replication*, H. Masai, M., Foiani, Eds. (Advances in Experimental Medicine and Biology Book Series, vol. 1024, Springer, 2017), pp. 259–272.
7. C. A. Seller, P. H. O'Farrell, *PLOS Biol.* **16**, e2005687 (2018).
8. R. Foti *et al.*, *Mol. Cell* **61**, 260–273 (2016).
9. R. T. O'Keefe, S. C. Henderson, D. L. Spector, *J. Cell Biol.* **116**, 1095–1110 (1992).
10. P. A. Zhao, T. Sasaki, D. M. Gilbert, *Genome Biol.* **21**, 76 (2020).
11. V. Dileep, D. M. Gilbert, *Nat. Commun.* **9**, 427 (2018).
12. T. Ryba *et al.*, *Genome Res.* **20**, 761–770 (2010).
13. K. Nishimura, T. Fukagawa, H. Takisawa, T. Kakimoto, M. Kanemaki, *Nat. Methods* **6**, 917–922 (2009).
14. K. Yoshida *et al.*, *Mol. Cell* **54**, 691–697 (2014).
15. P. Li *et al.*, *Nucleic Acids Res.* **45**, 12723–12738 (2017).
16. P. A. Zhao, Code for: Replication timing maintains the global epigenetic state in human cells, version 1, Zenodo (2021); https://doi.org/10.5281.zenodo.4606710.

ACKNOWLEDGMENTS

We thank R. Didier and B. Alexander of the FSU Flow Cytometry and Confocal Microscopy Facilities for their help with flow cytometry and fluorescence-activated cell sorting for this project. Thanks to A. Brown of the FSU Biological Science Core Labs and to Y. Yang and C. Vied of the FSU Translational Labs. Thanks to S. R. Westermann of SCIGRAPHIX for generating the model figure. Thanks to B. van Steensel, J. Phillips-Cremins, and P. Fraser for critical reading of the manuscript. **Funding:** This work was supported by NIH grant GM083337 to D.M.G., GM035463 to V.G.C., and GM085354 to D.M.G., S.D., and V.G.C. D.L. is supported by the Hong Kong Research Grant Council (ECS 26104216). T.B. is supported by the William C. and Joyce C. O'Neil Charitable Trust, Memorial Sloan Kettering Single Cell Sequencing Initiative. **Author contributions:** Conceptualization: K.N.K., P.A.Z., V.G.C., and D.M.G; Methodology: K.N.K., A.M.S., I.T., M.Z., L.P.W., S.H., T.N., and T.B.; Formal analysis: P.A.Z.; Investigation: K.N.K., X.L., T.S., D.A.B., and X.Z.; Writing – original draft: K.N.K., P.A.Z., and D.M.G.; Writing – review and editing: K.N.K., P.A.Z., X.L., V.G.C., and D.M.G.; Visualization: K.N.K. and P.A.Z.; Supervision: D.L., M.T.K., A.D.D., H.Z., S.D., V.G.C., and D.M.G.; Funding acquisition: D.M.G., S.D., and V.G.C. **Competing interests:** The authors declare no competing interests. **Data and materials availability:** All data are available on the Gene Expression Omnibus (GEO) #GSE160563. Code for data processing is available on Zenodo (*16*) and at https://github.com/oliviacamel/RIF1_KO_analysis.

SUPPLEMENTARY MATERIALS

science.sciencemag.org/content/372/6540/371/suppl/DC1
Materials and Methods
Figs. S1 to S20
Tables S1 to S5
References (*17*–*35*)
MDAR Reproducibility Checklist
Data S1 to S3

View/request a protocol for this paper from *Bio-protocol*.

30 December 2019; resubmitted 1 November 2020
Accepted 19 March 2021
10.1126/science.aba5545